

CP1: Investigation into the Feasibility of a Three Axis Interferometer for Biological Microscopy

Tom Wyatt

January 2012

Abstract

This report addresses the feasibility of using interferometry along three orthogonal axes in an attempt to attain images of biological samples at a better resolution than allowed by the diffraction limit. I examine the basic principles of interferometry and review recent techniques which have been developed to improve the resolution and versatility of interferometers. I then review recent uses of interferometry in biology and examine important techniques used when dealing with biological samples. Lastly I consider some initial questions which arise when extending these techniques to the concept of a three axis interferometer.

1 Introduction

Interferometry has long been an essential tool in optical microscopy. By interfering two electromagnetic waves, interferometric techniques are able to measure the relative phase of the waves. This allows measurement of the difference in distances travelled by the two waves up to a resolution of order picometres [1]. This is many orders of magnitude better than the normal limit in optical microscopy, as set by the diffraction limit and has led to the use of interferometers in a wide range of industrial and academic settings. In biology, in particular, interferometers have been used in many instances, from imaging tiny biological structures such as the eye of a housefly [2], to the detection of subnanometre displacements of a neuron membrane during the propagation of an action

potential [3, 4].

To date, the excellent resolution of interferometers has been limited to measurements in just one dimension. For example, take a large, flat surface lying in the xy -plane. Current interferometers are capable of accurately measuring subnanometre displacements of this surface in the z -direction (perpendicular to the plane), but are unable to measure the (x, y) coordinates of such a step to an accuracy greater than the diffraction limit allows. This limits the usefulness of interferometry in imaging and leaves a large proportion of biological structures beyond the resolution of optical microscopy.

This report explores the possibility of extending the resolution of interferometers into three dimensions. I examine the question as to whether or not interferometric measurements made by three orthogonal beams are capable of achieving greater than diffraction limit resolution whilst imaging a biological sample. Electron and scanning probe microscopy are already capable of resolutions much greater than the diffraction limit in optical microscopy, however, requirements in sample preparation, among other things, severely reduces the range of investigations suitable for their use. The benefits of having an optical microscopy technique with greater than diffraction limit resolution would be far-reaching, in particular because it would not require exogenous introduction of reporter chemicals or recombinant proteins such as fluorescent markers.

This report is organised as follows. In section 2 the principles of interferometry are examined and explained. Recent developments in interferometric techniques are then reviewed. Section 3 goes on to

explain how interferometry is applied to biological measurements and reviews recent applications of interferometry in biology. In section 4 I address the subject of interferometry along three axes and begin to explore whether the concept would indeed allow sub-diffraction limit resolution.

2 Interferometric Methods

In the broadest sense, optical interferometry is the combining of electromagnetic waves in order to obtain information from those waves. It uses the principle of superposition: that the amplitudes of electromagnetic waves add vectorially when interfered. The relative phase of the combined waves dictates whether this superposition leads to constructive or destructive interference and in this sense the signal wave can convey information regarding phase [5].

An important condition for interference is coherence. This is a property of one or more waves, first described by Thomas Young [6] which, by definition, is the degree to which two waves are able to interfere. Two waves with a constant phase difference with respect to one another are said to be completely coherent and can interfere maximally. A wave emitted from a single source has two types of coherence: spatial and temporal. Spatial coherence describes the degree of coherence between the wave at different points in space. Similarly, temporal coherence describes the coherence between two sections of the wave, taken from two different points in time. As an example, a source which emits light in many short bursts, occurring at random intervals, will have low temporal coherence. Coherence is important in interferometry not only because it allows the required interference to occur, but conversely, because reducing the coherence of the source waves allows selectivity in which parts of the waves are used. This will be demonstrated later in this section.

Two classes of interferometric technique exist: homodyne and heterodyne detection [5]. In the homodyne case, the waves which are combined originate from the same source and any differences between the waves at detection are a consequence of unknowns in the experiment. In some instances, how-

ever, it is advantageous to alter one of the waves in a known manner and this is called heterodyne detection. To illustrate this important technique, take two waves: $E_1 \cos(\omega_1 x)$ and $E_2 \cos(\omega_2 x + \phi)$. Wave 2 has been created by shifting the frequency of wave 1 by a known amount, $\omega_2 - \omega_1$ and an unknown phase difference, ϕ , has been introduced. Waves 1 and 2 have amplitudes E_1 and E_2 respectively. When these waves are interfered and intensity, I , is measured, the result has the form:

$$\begin{aligned} I &= E_1^2 \cos^2(\omega_1 x) + E_2^2 \cos^2(\omega_2 x + \phi) \\ &\quad + E_1 E_2 \cos(\omega_1 x) \cos(\omega_2 x + \phi) \\ &= \frac{1}{2} (E_1^2 + E_2^2) + \frac{1}{2} E_1^2 \cos(2\omega_1 x) \\ &\quad + \frac{1}{2} E_2^2 \cos(2\omega_2 x + 2\phi) \\ &\quad + E_1 E_2 \cos((\omega_2 - \omega_1)x + \phi). \end{aligned} \quad (1)$$

The last term is a wave oscillating at the slower frequency of $\omega_2 - \omega_1$. In many cases this slow oscillation facilitates the analysis of the signal. Here, for instance, the phase difference ϕ appears in the slower oscillation as well as the faster oscillating components. This can make ϕ easier to measure as it has effectively been amplified.

Figure 1 depicts the simplest case experimental setup for measuring a small displacement of length ΔL in a sample surface, using homodyne detection. Light of wavelength λ , from a coherent source S , is split into two at the beam splitter BS . One part of the beam travels to a reference mirror a distance L away and is reflected back to the beam splitter while the other part of the beam travels to a sample which is a distance $L + \Delta L$ away, before also being reflected back to the beam splitter. At the beam splitter the beams recombine and the signal is detected by a photodetector. The total difference in path length travelled by the two beams is $2\Delta L$ so (assuming constant refractive index) the phase difference, $\Delta\phi$, between the beams is:

$$\Delta\phi = \frac{2\pi}{\lambda} 2\Delta L = 2k\Delta L, \quad (2)$$

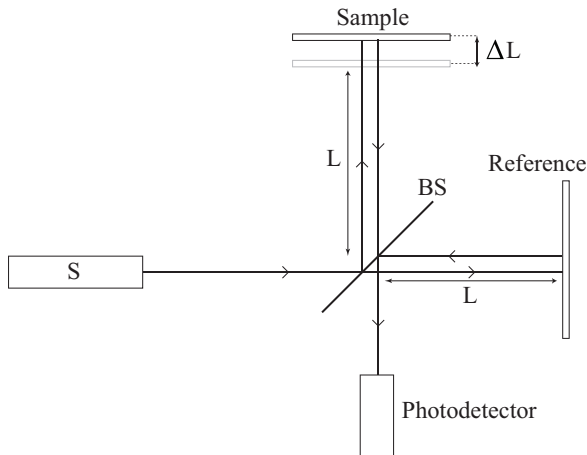


Figure 1: A simple interferometric experiment using homodyne detection in a Michelson interferometer. ΔL is the difference in lengths of the two interferometer arms, BS is a beam splitter and S is a coherent source.

where k is the wavenumber. When the waves interfere the resulting intensity depends on the relative phase and therefore on ΔL . It is at a maximum for $\Delta L = 0$ and approaches zero towards $\Delta L = \frac{\lambda}{4}$, i.e. when $\Delta\phi = \pi$. This shows that a resolution of $\frac{\lambda}{4}$ (a ‘subdivision factor’ of $\frac{1}{4}$) is possible and this can be improved with sensitive intensity measurements.

One important caveat to this example concerns phase ambiguity. It is impossible to distinguish between a phase change of $\Delta\phi$ and one of $\Delta\phi + 2\pi$ and this causes an uncertainty in ΔL of $\pm n\frac{\lambda}{2}$, where n is any integer. To reduce this ambiguity, some experiments use a source with low temporal coherence [7]. This means that if there is too large a delay between the two beams they will no longer be coherent and so will be unable to interfere, thus reducing the ambiguity.

The interferometer in figure 1 is a Michelson interferometer. This simple configuration is employed in many situations but there are a large number of alternate arrangements in use, each with their own advantages. Two are depicted in figure 2. The first, figure 2 a), is the Mirau interferometer. It is more compact than the Michelson and contains just one objective lens, meaning it is not necessary to accu-

ately match two lenses. Another important advantage over the Michelson is that more of the optical paths of the two beams can share the same path, which reduces phase noise. The central reference mirror, however, obscures a certain portion of the image. Dobroiu et al. [8] have designed a variation on the Mirau interferometer which they call the coaxial Mirau interferometer. It overcomes the problem of the central obscuration and allows for a high degree of miniaturization.

Figure 2 b) shows a Mach-Zehnder interferometer. Topologically it can be thought of as an unfolded Michelson. Although it is the least compact of the three, it is useful for situations where transmission through a sample is convenient, rather than reflection from it.

Equation 2 above demonstrated how a subdivision factor of $1/4$ is achieved in the simplest case. Greater resolutions, however, have been achieved using a myriad of methods. Lu et al. [9] used nonsymmetrical double gratings to obtain a subdivision of $1/24$. An electronic technique called phase-shifting interferometry was used by Onodera et al. [10] to achieve a subdivision of $1/1000$ and CCDs have recently been used by Chen et al. [11] to reach a factor of $1/2000$. As an example I will describe in detail the particularly impressive ‘Dual-wavelength’ technique introduced by Chen et al. [1].

As an example the particularly impressive ‘Dual-wavelength’ technique introduced by Chen et al. [1] will now be described in detail. This method achieved a subdivision factor of $1/440000$ and experimentally attained a resolution of better than 50 pm. Their experimental setup is shown in figure 3. The method uses of two orthogonally polarized beams (1 and 2) of wavelength λ_1 and λ_2 , respectively. Orthogonally polarised light is used because such beams don’t interfere and can be easily separated by polarizing beam splitters. Their apparatus effectively contains two Michelson interferometers, one for each of the beams. Beam 1 is split so that half propagates to the reference corner cube (RCC) and half to the polarizing beam splitter (PBS), which is configured to only reflect this beam. The two parts of beam 1 therefore only accumulate the relative phase difference $\phi_1 = 2\pi(L/\lambda_1)$, where L is a path difference in the

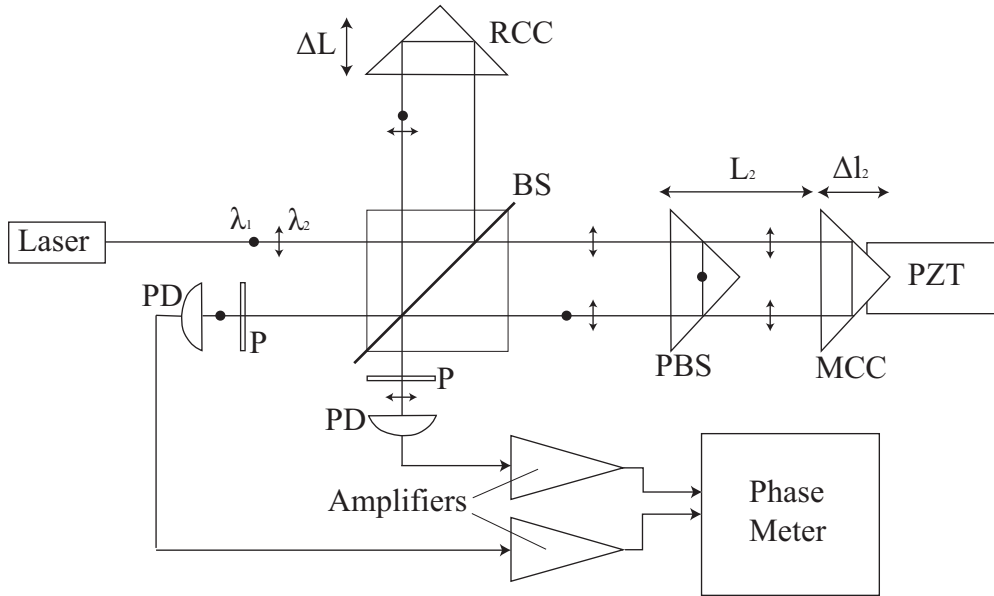


Figure 3: The ‘Dual-wavelength’ interferometer introduced by Chen et al. BS is a beam splitter, PZT is a piezoelectric transducer, P are polarizers, PD are photodetectors, other abbreviations are defined in the text.

reference arm.

Beam 2 is split so that half propagates to the RCC while the other half passes the PBS, travelling an extra L_2 compared to beam 1 to be reflected by the measurement corner cube (MCC). The relative phase difference introduced between the two parts of beam 2 is therefore $\phi_2 = 2\pi \left(\frac{L}{\lambda_1} - \frac{L_2}{\lambda_2} \right)$. The total phase difference, $\Delta\phi$, between beams 1 and 2 is measured by a time interval analyzer and is given by

$$\Delta\phi = 2\pi \left(\frac{L}{\lambda_s} - \frac{L_2}{\lambda_2} \right),$$

where $\lambda_s = \lambda_1\lambda_2/|\lambda_1 - \lambda_2|$ is named the ‘synthetic wavelength’ and is clearly longer than either λ_1 or λ_2 . When the MCC is moved a small distance Δl_2 the phase difference $\Delta\phi$ becomes $\Delta\phi'$, which is given by

$$\Delta\phi' = 2\pi \left(\frac{L}{\lambda_s} - \frac{L_2 + \Delta l_2}{\lambda_2} \right). \quad (3)$$

Measurement of $\Delta\phi'$ would correspond directly to a measurement of Δl_2 if L and L_2 were known. Clearly,

however, they will not be known to the degree of precision that Δl_2 is wished to be measured to. Therefore, yet another path difference of ΔL is introduced. This is inserted into the reference arm so affects both beams 1 and 2, however, the phase difference produced in each is different, depending on wavelength as in equation 2. ΔL is then varied until $\Delta\phi'$ is equal to the original phase difference $\Delta\phi$. Inserting $L \rightarrow L + \Delta L$ into equation 3 and setting $\Delta\phi = \Delta\phi'$ yields the condition

$$\Delta l_2 = \frac{\lambda_2}{\lambda_s} \Delta L.$$

Since the wavelengths can be chosen such that $\lambda_s \gg \lambda_2$, a large measured movement ΔL (with a correspondingly large uncertainty) is used to measure Δl_2 to a high degree of accuracy. Chen et al. use a dual-longitudinal-mode laser with $\lambda_2 = 632.8$ nm with a frequency difference between the two modes of $\Delta\nu = 1070$ MHz which gives a subdivision factor $K_{div} = \lambda_2/\lambda_s \approx 1/440000$. This allows the better than 50 pm resolution quoted above.

3 Interferometry in Biology

The interferometers so far reviewed were built with the purpose of demonstrating a novel interferometric technique. Therefore they have used ‘ideal’ samples such as highly reflective, smooth surfaces. This section explains how and why interferometry is used on biological samples and reviews recent developments in the field.

A common problem in biological optical microscopy is low contrast between features of interest. This is due to a large proportion of biological material being colourless and transparent [12] and results in the need to use dyes to increase contrast. It is often the case that such features, despite being colourless and transparent, do have varying refractive indexes. This produces the reflections and/or changes in optical path length¹ required for interferometry, making it more suitable than other methods such as bright field microscopy.

Another, less obvious, advantage that interferometry has over other microscopy techniques is that the measured response in interferometry is proportional to the amplitude of the received signal as opposed to the intensity [7]. This is an inherent property of interferometry as can be seen in equation 1. If, in this simple heterodyne detection case, the amplitudes E_1 and E_2 had started at unity, then upon reflection they would become $\sqrt{R_1}$ and $\sqrt{R_2}$, the square root of the reflectances of the reference and sample mirror respectively. By using a strong mirror it is simple to make $R_1 \approx 1$. This leaves the detected, interference part of the combined wave: $R_2 \cos((\omega_2 - \omega_1)x + \phi)$. This is clearly proportional to amplitude of signal, not intensity and in situations where contrast is low this produces a stronger output.

For these two reasons, as well as the exquisite, one dimensional resolution, interferometry has been used extensively in biology. It has been used to measure changes in cell thickness of a chick embryo cardiomyocyte during beating [13], to image the surface of the

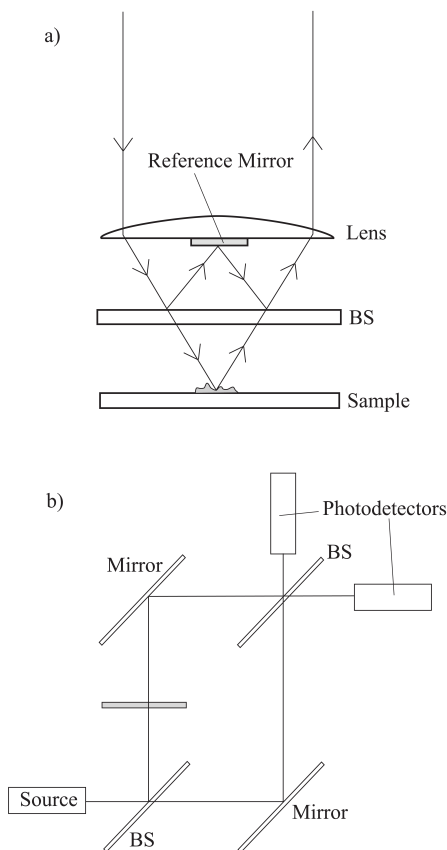


Figure 2: a) depicts a Mirau interferometer, b) depicts a Mach-Zehnder interferometer. In both BS are beam splitters.

¹Optical path length, OPL , is defined as $OPL = nd$ where n is the refractive index of the medium and d is the distance travelled by the light. It is used to take into account the effect that the refractive index of the medium has on the phase of the light, as well as the distance travelled.

compound eye of a housefly [2], to measure swelling of intestinal epithelial cells in hyper- and hypotonic growth media [14] and to measure surface motion in lobster and cray-fish nerve bundles [3, 4].

The first issue encountered in biological settings is that of reflectivity. Having argued that many features in biological samples do have varying refractive indexes, the question remains as to whether these refractive differences are great enough to produce a detectable reflection. The fraction of the wave power that is reflected at the interface between media with different refractive indices depends on the angle of incidence and polarization of the light and can be calculated using Fresnel's equations [15]. For normal incidence, as used in many interferometers, the Fresnel equations simplify to

$$R = \left(\frac{n_1 - n_2}{n_1 + n_2} \right)^2,$$

independent of what the polarization is, where R is the fraction of wave power that is reflected and n_1 and n_2 are the refractive indexes before and after the interface, respectively. A typical refractive index of a cell is $n_{cell} \approx 1.37$ [16] and air has $n_{air} \approx 1$. Therefore, at this interface, only approximately 2.4% of the power is reflected. This demonstrates that a large portion of the power is lost which is problematic, however, as described above, the situation is helped by interferometric signals being proportional to the amplitude, not the intensity. It is often desirable to image cells whilst in growth media and as might be expected, this often has a refractive index much closer to that of a cell. A typical value is $n_{growth} \approx 1.33$ [16], meaning just $\sim 0.02\%$ is reflected.

Despite these seemingly low reflectances, many interferometric investigations of biological samples have been successfully carried out without the need to modify the sample in any way [3, 4, 14]. Such experiments rely on sensitive detection and use high intensity sources. In other cases the biological sample and its surrounding medium created an interface which reflected strongly, such as the reported 10% reflection from the housefly eye imaged by Fang-Yen [2]. In yet other cases, however, samples have been modified by applying highly reflective materials on

the sample surface [17, 18]. Hill et al. [18], for example, deposited gold dust particles on the surface of Crayfish axon which increased reflection, but unfortunately also decreased the fraction of light which reflected specularly. This technique also overcomes an issue often ignored in other experiments: the changing of the optical properties of the cell itself during a process of interest (in this case the action potential).

Another issue in biological settings involves the restrictions that the shape and size of the sample (and its necessary environment) pose. A great variety of situations of this kind arise. Cells under inspection may need to be imaged whilst immersed in growth media, they may form just a small section of a larger whole or they may be neurons that must be attached to electrodes for stimulation. Having constant access to the sample during the experiment may also be a necessity. Such restrictions often motivate significantly different arrangements of interferometers from ones described so far. Additionally, as more applications for interferometry are discovered, configurations are being devised which are compact and simple enough for clinical use.

Figure 4 depicts the interferometer created by Choma et al. [13] to measure the dynamics of beating cardiomyocytes. Here, space is saved by mounting the sample cells on one side of a coverslip and using the interface with air at the opposite side for the reference reflection. A key advantage is that, as can be seen in the diagram, the path of the reference and sample beams is identical for almost the entire length, meaning that any phase noise in the interferometer is likely to be shared by both beams and therefore cancel.

The probe interferometer developed by Fang-Yen et al. [?] is another example of a novel interferometer, devised for biological use. It is depicted in figure 5. Fang-Yen et al. cite two main issues which lead them to this design. Firstly, again, is finding room for a reference surface close to the sample. This is particularly a problem when access to the sample is needed during measurement or if this reference surface needs to be adjusted due to movement or reorientation of the sample.

The second problem concerns the numerical aperture of the objective lens. Numerical aperture, NA ,

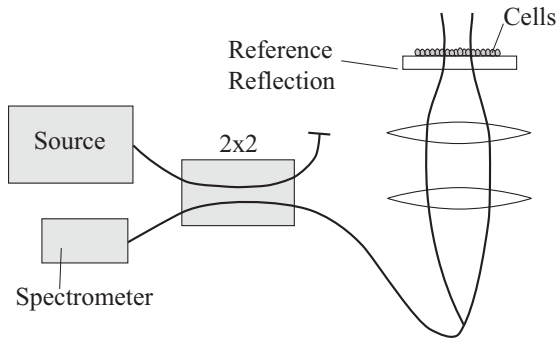


Figure 4: The spectral-domain interferometer of Choma et al. [13].

is a measure of the light collecting ability of a particular lens and is given by

$$NA = n \sin \theta_0 \quad (4)$$

where n is the refractive index of the medium surrounding the lens and θ_0 is the angle as shown in figure 6. It is usually desirable to have a numerical aperture close to the maximum value of n since transverse resolution scales as λ/NA . However, in this case a competing factor is that of depth of field. Depth of field describes the distance along the optic axis of the lens over which the focal point extends and can be shown to be $\sim \lambda/NA^2$. In an interferometer it is desirable, but not essential, to have both the reference and sample surface within the focal point so as to avoid power loss in either one. Clearly this is hard to achieve whilst maintaining a numerical aperture of $NA \approx n$.

The probe interferometer in figure 5 solves both these issues by using for the reference surface the cleaved end of the optical fibre which transmits all emitted and received light. The reflection is caused by the refractive index difference between the fibre and the surrounding air. The light emitted by the fibre end is then focused by the gradient indexed microlens. This lens can thus have a high numerical aperture without affecting the reference reflection.

The solutions described so far in this section have enabled interferometry to make important biological discoveries and allow for exciting possibilities

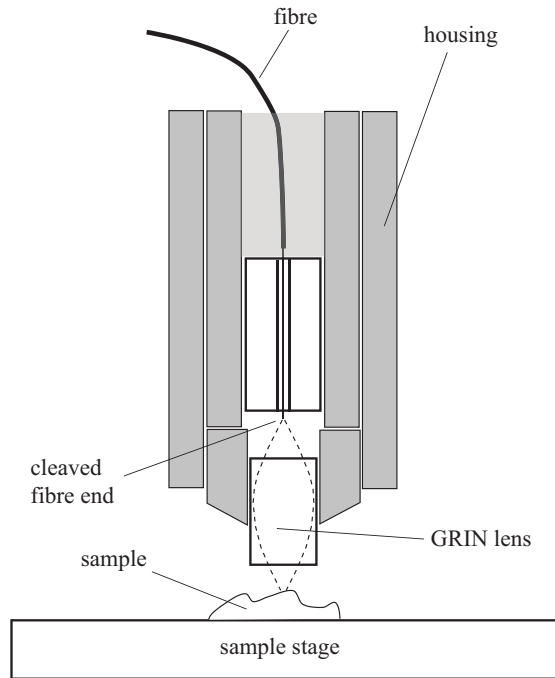


Figure 5: The probe interferometer design introduced by Fang-Yen et al. [2]. The cleaved fibre end is used as a reference surface.

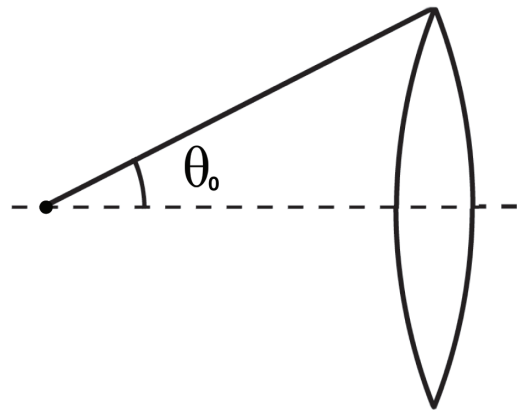


Figure 6: The numerical aperture of a lens is given by $n \sin(\theta_0)$, where n is the refractive index.

in the future. The measurement of the swelling of neurons during the action potential is certainly one of the most interesting applications. Interferometry provided the first non-invasive measurements of the swelling [4], demonstrating that previous observations were not due to perturbations caused by the invasive measurement methods. Interferometry was also shown to be capable of measuring the magnitude of the swelling to greater accuracy than had been achieved previously. All of this makes interferometry an exciting candidate for many fundamental nerve investigations and for non-contact detection of many neuropathies, with the possibility of use in a clinical setting.

For the sake of focus, this section of the report has dealt with just one class of interferometric techniques in biology: in all cases discussed reflections from a biological surface were interfered with those from a reference surface to gain information about the position of that surface. There are many other roles that interferometry plays in biology. One class of method observes the dynamics of biomolecules that are too small to resolve directly by binding them to larger reflective objects. An interferometer is then used to track the motion of the larger object. For example, Svoboda et al. [19] attached silicon beads to the biological motor kinesin and used interferometry to ascertain that it moved along microtubules in discrete 8 nm steps. Interferometers also play a crucial role in the area of biosensing [20, 21, 22]. Here interferometers are used to measure small changes in refractive index when target molecules bind to receptors on a surface. All such techniques have some degree of relevance to this investigation since a three axis interferometer, with subnanometre resolution in three dimensions, would instantly expand the scope of such methods.

4 Three axis Interferometry

Informed by the review of interferometric techniques in the previous two sections, the possibility of combining three interferometers in order to obtain greater than diffraction limit resolution in all three dimensions is now considered. This simple concept pro-

poses that, since current interferometers are able to obtain such remarkable resolution in one dimension, the combination of three interferometers, aligned orthogonally to each other, may be able to provide similar resolution in all three dimensions.

In order to direct three orthogonal beams onto a planar sample, the three axis interferometer will need each of the beams directed obliquely at the sample. The three beam's directions can be thought of as the three sides of a cube, which meet at one corner. If arranged symmetrically, the angle made by this beam and the sample plane is given by $\arcsin(1/\sqrt{3}) \approx 35^\circ$. It may be necessary to choose other values for this angle, so from here on this is referred to as θ_i .

A preliminary question is that regarding light collection. Standard interferometers collect light from the direction perpendicular to the sample plane, the same direction that the sample is illuminated from. Here, since the sample is illuminated obliquely, it is not so clear cut what collection angle should be chosen. Figure 7 shows two obvious choices for the collection angle, which is denoted θ_c . One option is to collect from the same angle as the sample is illuminated from, this is θ_{c1} in the figure. This seems a sensible choice: light reflected diffusely from the sample can be collected using the same unit as used for illumination. One drawback is the loss of light reflected specularly from planar sections of the sample. In some cases this may account for a large proportion of the signal. An angle θ_{c2} may be chosen such that specularly reflected light is collected but this too has a major drawback. Features such as that shown in the figure block sections of the sample from view. The shading in the figure shows areas which this arrangement cannot collect information from. This will naturally have a detrimental affect on the resolution.

The choice of collection angle fundamentally changes the effect that a feature such as that shown in figure 7 has on the distribution of phase in the received light. A truly informed choice cannot be made until the full theory of the microscope has been fully analysed and therefore has to be left as an important question to be addressed in future work.

Figure 8 depicts three possible configurations for the three axis interferometer. Each example is closely

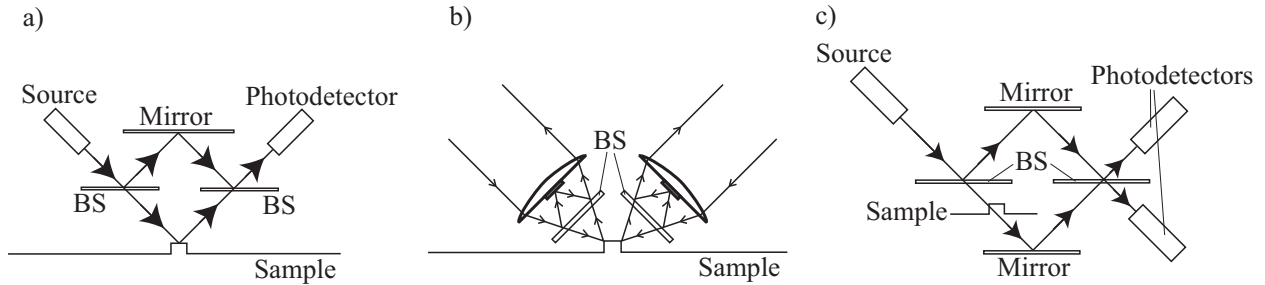


Figure 8: Three possible arrangements for the interferometers which make up the three axis interferometer. a) is equivalent to the standard Michelson Interferometer, b) to the Mirau and c) to the Mach-Zehnder

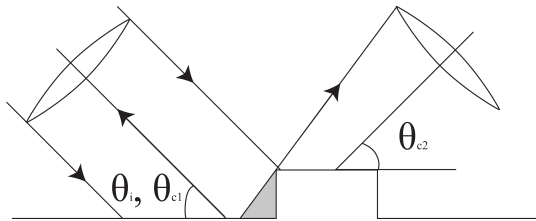


Figure 7: Two possible choices for the collection angle in the three axis interferometer.

related to one of the forms discussed in section 2: a) corresponds to the Michelson interferometer, b) to the Mirau and c) to the Mach-Zehnder. In each case the full, three axis interferometer is made from three copies of a diagram, rotated to angles of 120° to each other. It can be seen that the standard interferometers require little serious amendment, so few engineering difficulties should arise. The relative merits of each design follow the same arguments as their standard counterparts. For instance, again the Mach-Zehnder is the least compact, the Michelson a little more so and the Mirau the most compact. Still the Mirau suffers from the central obscuration due to the reference mirror. It is worth noting that in the Michelson and the Mach-Zehnder interferometers the mirrors above and below the sample can be shared by each of the three systems that make up the entire three axis device.

At this stage, the most important question regarding the three axis interferometer is whether or not it will genuinely be capable of greater than diffraction limit imaging. To answer this, a full theoretical treatment of the interferometer is required. Using standard techniques of theoretical optics it should be possible to predict the response of the interferometer to simple sample geometries. Further analysis will then be required to understand how, from this predicted signal, features of the sample are identified and to what resolution. A key part to this work will be to understand how the signals from the three different axes are combined to give a three dimensional result. The very first steps in this theoretical process were taken and are described in what follows.

The layout of the problem is shown in figure 9. The sample in question is a single step of height h , the simplest possible starting point. Light of wavelength λ is incident on this sample at angle θ_i . This, for example, may be laser light with a Gaussian profile and is denoted $u(x)$. Reflected light is collected with a lens whose optic axis is at angle θ_c from the sample plane. An identical situation appears at the reference mirror except with no step. The approach taken uses Fourier analysis in a similar way as in more basic diffraction problems. It can be explained best in light of Abbe's theory of imaging.

Abbe's theory of imaging describes how information regarding the spatial variation of an object is carried by waves whose wavelength is of the same size as that spatial variation. Hence, in an optical system which uses light of wavelength λ , the mini-

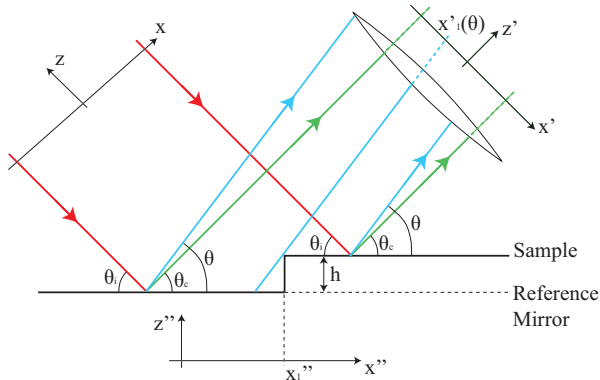


Figure 9: A step function being imaged by an interferometer along with the various quantities used to derive the interferometer's response.

imum size of variation that can be imaged, i.e. the resolution, is of order λ . This is another formulation of the diffraction limit. Abbe theory also explains how high resolution information is carried by waves which travel at a large angle to the optical axis since, in spatial frequency space (also known as k -space), these waves have a larger component in the image plane. Therefore, resolution is also limited by the inability of the lens to collect these high angle waves.

As a first step, the form of the incident wave is derived for the point where it reaches the sample surface. This is achieved by calculating the phase differences which occur due to the geometry of the sample and the angle of the incident light.

I then Fourier transformed the waveform at the sample surface, to decompose it into its Fourier components. This was done whilst taking into account the fact that waves leaving at different angles (i.e. the different Fourier components) accumulate different phases due to their angle and the geometry of the sample. A Fourier component from the sample $U_s(k'_x)$ is then given by

$$U_s(k'_x) = \int u_s(x', \theta) e^{ik \sin(\theta - \theta_c) x'} dx' \quad (5)$$

with

$$u_s(x', \theta) = \begin{cases} u\left(x' \frac{\sin \theta_i}{\sin \theta_c}\right) \times \\ \exp\left(ikx' \left[\frac{\cos \theta_i}{\sin \theta_c} - \cot \theta\right]\right) & x' < x'_1 \\ \\ u\left(x' \frac{\sin \theta_i}{\sin \theta_c}\right) \times \\ \exp\left(ikx' \left[\frac{\cos \theta_i}{\sin \theta_c} - \cot \theta\right] - h \cot \theta_i\right) & x' > x'_1 \end{cases}$$

where unprimed coordinates are incident beam coordinates and primed are the collection angle coordinates, as shown in the figure. The transformation between these coordinates can be shown to be $x = x' \frac{\sin \theta_i}{\sin \theta_c}$. $x'_1(\theta)$ is the point in the collection coordinates where the step in the sample occurs and is given by

$$x'_1(\theta) = (x''_1 - h \cot \theta) \sin \theta$$

where x''_1 is the position of the step in the sample coordinates. It is ultimately a small chance in this value which we hope to measure. The same steps are used on the reference mirror part of the interferometer which gives Fourier components of the same form as equation 5 but with u_s replaced with u_r , which is given by

$$u_r(x', \theta) = u\left(x' \frac{\sin \theta_i}{\sin \theta_c}\right) \exp\left(ikx' \left[\frac{\cos \theta_i}{\sin \theta_c} - \cot \theta\right]\right).$$

To retrieve the final signal detected by the interferometer, the sample and reference Fourier components are summed together and Fourier transformed again. This time, however, only the Fourier components which can be collected by the lens are included in the transform to give the true, degraded image that is detected. This final detected signal $u_d(x')$ is

given by

$$u_d(x') = \dots$$

$$\int_{k'_{xmin}}^{k'_{xmax}} [\int (u_s(x', \theta) + u_r(x', \theta)) e^{ix'k \sin(\theta - \theta_c)} dx'] e^{ix'k \sin(\theta - \theta_x)} dk'_x. \quad (6)$$

where the k-space integral limits are given by

$$k'_{xmax} = k \sin \theta_0$$

and

$$k'_{xmin} = -k \sin \theta_0$$

where θ_0 is related to the numerical aperture as in equation 4.

This result cannot be solved analytically and so the starting point for further work will be to find numerical solutions to equation 6. From this it should be possible to learn what resolution the interferometer is capable of.

As a final remark for this section, it is interesting to note two possibilities which arise from illuminating the sample obliquely. Firstly, if the cells can be contained in a medium with a higher refractive index than the cells themselves, total internal reflection could be used to ensure 100% reflection from the cells, thus strengthening the signal. Secondly, an experiment could be arranged to make use of the Brewster angle. This is the angle at which, at the interface between two materials of different refractive index, all light of a certain polarisation is transmitted. If the cells must be kept in a growth medium, choosing the Brewster and the correct polarisation will allow 100% transmission into the growth medium, to the sample cells.

5 Conclusion

This report has aimed to explore the feasibility of extending to three dimensions the excellent resolution achieved in one dimension by interferometric techniques in biology. To this end I have examined the fundamental principals of interferometry and reviewed a number of common techniques that are used

to make interferometers both more accurate and more versatile. I have shown how interferometry is applied to biology, reviewing a variety of methods used to deal with the problems the biological setting introduces.

Finally, a number of questions about the concept and execution of a three axis interferometer have been posed and the first steps towards their solutions have been taken. Considerations involving light collection were discussed and some possible configurations for the interferometer have been compared. The response of the interferometer to a simple 'step function' from an oblique angle was derived as a first step towards theoretically demonstrating the ability (or otherwise) of a three axis interferometer to resolve structures at a resolution greater than the diffraction limit.

Whether or not the concept of a three axis interferometer will be capable of increased resolution is still an entirely open question. The theory of the interferometer, which I began to examine, remains to be derived as was briefly laid out in section 4. If this theory suggests that better than diffraction limit resolution is indeed achievable with the interferometer, the next step is to obtain experimental evidence of this. A good candidate for imaging is the etched biological samples that are used for (and can be compared to the images from) electron microscopy. If such experiments are successful the microscope will have great potential to dramatically broaden the scope of biological investigation.

References

- [1] B. Chen, X Cheng, D. Li, *App. Opt.* **41**, 5933-7 (2002).
- [2] C. Fang-Yen, M. C. Chu, H. S. Seung, R. R. Dasari and M. S. Feld, *Rev. Sci. Instrum.* **78**, 123703 (2007).
- [3] T. Akkin, D. P. Davé, T. E. Milner and H. G. Rylander III, *Opt. Exp.* **12**, 2377-86 (2004).
- [4] C. Fang-Yen, M. C. Chu, H. S. Seung, R. R. Dasari and M. S. Feld, *Opt. Lett.* **29**, 17 (2004).

- [5] S. Tolansky, *Introduction to Interferometry*, (Longman, 1973).
- [6] G. Peacock, *Life of Thomas Young*, (The British Library, 1855).
- [7] G. Kino and S. Chim, *Appl. Opt.* **26**, 3775-83 (1990).
- [8] A. Dobriou, H Sakai, H Ootaki, M. Sato and N. Tanno, *Opt. Lett.* **27**, 1153 (2002).
- [9] H. Lu, J. Cao, S. Su and G. Tang, *SPIE* **4077**, 40-43 (2000).
- [10] R. Onodera and Y. Ishi, *Appl. Opt.* **33**, 5052-5061 (1994).
- [11] B. Chen, D. Li and R. Zhu, *Opt. Technique* **27**, 223-225 (2001).
- [12] B. Alberts, A. Johnson, J. Lewis, M. Raff, K. Roberts and P. Walter, *Molecular Biology of the Cell*, (Garland Science, 2008).
- [13] M. Choma, A. Ellerbee and C. Yang, *Opt. Lett.* **30**, 1162-4 (2005).
- [14] C. Yang, A. Wax, M. Hahn, K. Badizadegan, R. Dasari and M. Feld, *Opt. Lett.* **26**, 1271-3 (2001).
- [15] E. Hecht, *Optics*, (Pearson, 2003).
- [16] B. Kemper, S. Kosmeier, P. Langehanenberg, G. von Bally, I. Bredebusch, W. Domschke and J. Schnekenburger, *J. of Biomed. Opt.* **12**, 054009 (2007).
- [17] M. Nokes, B. Hill and A. Barelli, *Rev. Sci. Instrum.*, **49**, 722 (1978).
- [18] B. Hill, E. Schubert, M. Nokes, R. Michelson, *Science* **196**, 426-428 (1977).
- [19] K. Svoboda, C. Schmidt, B. Schnapp and S. Block, *Nature* **365**, 721-727 (1993).
- [20] X. Fan, I. White, S. Shopova, H. Zhu, J. Suter and Y. Sun, *Analitica Chimica Acta* **620**, 8-26 (2008).
- [21] V. Lin, K. Motesharei, K. Dancil, M. Sailor and M. Ghadiri, *Science* **278**, 840 (1997).
- [22] M. Varma, H. Inerowicz, F. Regnier and D. Nolte, *Biosens. Bioelectron.* **15**,1371 (2004).